Materials Science & Engineering C 112 (2020) 110895

Contents lists available at ScienceDirect

Materials Science & Engineering C

journal homepage: www.elsevier.com/locate/msec

Rifampicin nanocrystals: Towards an innovative approach to treat tuberculosis

Katherine Jasmine Curo Melo[a], Mirla Anali Bazán Henostroza[a], Raimar Löbenberg[b,*], Nádia Araci Bou-Chacra[a,*]

[a] Faculty of Pharmaceutical Sciences, University of Sao Paulo, Sao Paulo, Brazil
[b] Faculty of Pharmacy and Pharmaceutical Sciences, University of Alberta, Edmonton, Canada

ARTICLE INFO

Keywords:
Rifampicin
Nanosuspension
Nanocrystals
Wet bead milling

ABSTRACT

Tuberculosis (TB) is one of the top ten causes of death worldwide and a leading cause of death in HIV patients. Rifampicin (Rif), a low water-soluble drug, is a critical first-line treatment and the most effective drug substance for therapy of drug-susceptible TB. However, Rif has high interindividual pharmacokinetic variability, mainly due to its highly variable absorption caused by its poor solubility. Drug nanocrystals are a promising technology to overcome this variability by increasing the surface area. This strategy allows for increasing the dissolution rate and improving the bioavailability of this BCS class II drug. In this study, Rif nanocrystals were prepared by a wet-bead milling method. A 3-factor, 3-level Box-Behnken design was used to investigate the independent variables: the concentration of rifampicin, the concentration of the stabilizing agent (Povacoat® type F), and the mass of zirconia beads. Two optimized formulations, F1-Rif and F2-Rif, were characterized by determining their particle size and size distribution, morphology, crystal properties, and antimicrobial activity. Differential scanning calorimetry (DSC) and powder X-ray diffraction (PXRD) revealed that rifampicin's polymorph II crystal structure was unchanged. The reduced particle size of < 500 nm (100-fold decrease) increased the saturation solubility and dissolution rate up to 1.74-fold. The novel polymer, Povacoat®, demonstrated to be a suitable stabilizer to maintain the physical stability of nanosuspensions over two years. The Rif nanocrystals showed antimicrobial activity (0.25 μg/mL) not significantly different from standard rifampicin powder. However, the low cytotoxicity of the nanosuspensions in HepG2 cells was determined. When compared to the commercial product, the nanosuspension increased the rifampicin concentration 2-fold. In conclusion, the Rif nanosuspension allows half the needed volume of administration, which might increase compliance among children and elderly patients throughout the long-term treatment of TB.

1. Introduction

Tuberculosis (TB) is a millenary global disease caused by *Mycobacterium tuberculosis*, first described by Dr. Koch [1]. Despite significant advances in science and technology, this disease still represents a significant global Public Health risk. TB is one of the top ten causes of death worldwide and a leading cause of death in HIV patients [2]. Rifampicin (Rif), a broad-spectrum antibiotic, belongs to the first line of treatment. Rif is a Class II drug according to Biopharmaceutical Classification System (BCS), with low water solubility and high permeability, showing variable bioavailability due to its in vivo dissolution and is subject to food effects [3,4]. Additionally, Rif has seven crystalline forms [5]; the polymorph II, which presents higher water solubility, is metastable, and it is the commonly marketed form used in pharmaceutical products [6].

Particle size reduction into the nanometer scale is a promising approach to increase the dissolution of hydrophobic drugs [7,8]. Nanocrystals are matrix-free drug particles often stabilized by surfactants, polymers, or a mixture of both. In general, the particles are below 1000 nm in size, typically between 200 and 500 nm [7,9]. The biphasic system of stabilizer and crystals is called a nanosuspension. Due to the increased surface area, this strategy allows besides increasing the dissolution rate an adhesion of the poorly water-soluble drugs to the gut wall, improving the bioavailability of class II drugs [10].

Literature describes two approaches to produce nanocrystals: bottom-up and top-down methods. Top-down technology consists of breaking large particles into small sizes using mechanical grinding (wet media milling) and high-pressure homogenization or a combination of

* Corresponding author.
E-mail addresses: raimar@ualberta.ca (R. Löbenberg), chacra@usp.br (N.A. Bou-Chacra).

https://doi.org/10.1016/j.msec.2020.110895
Received 14 August 2019; Received in revised form 28 February 2020; Accepted 21 March 2020
Available online 23 March 2020

both [11–14].

Miniaturized wet-bead milling is a novel approach for screening formulation variables and process parameters (time and stirring speed). The system consists of a milling chamber (glass recipient) filled with zirconia beads, drug substance, dispersion media (stabilizer in aqueous solution), and two or three magnetic stirring bars placed vertically. This system is agitated by a magnetic stirrer plate at high speed [15,16]. This simple low-cost method is performed in small volumes, which provides advantages in early drug development. Besides, this procedure may predict results of high-energy milling at pilot scale and identifies suitable preparation parameters [15,17].

The stabilizing agents (surfactants and polymers) play an important role in particle size reduction and stability of nanosuspensions. Daido Chemical Corporation developed a novel polymer with a molecular mass of 40,000, Povacoat® type F (POVA), (polyvinyl alcohol/acrylic acid/methyl methacrylate copolymer). This pharmaceutical excipient was initially developed as a film-coating agent and wet granulation binder. However, recent studies revealed the use of Povacoat® as a stabilizer to prevent aggregation of nanocrystals [18–21].

In this study, Rif nanocrystals were developed. Their low water solubility was improved by reducing the particle size. The parameters such as particle size, distribution, zeta potential, and morphological characterization of nanocrystals were assessed. Additionally, the physical stability of nanosuspension (two years), the in vitro anti-microbial efficacy and cytotoxicity were evaluated.

2. Materials and methods

2.1. Materials

Rifampicin (Rif) (purity 98%) and micronized rifampicin commercial suspension (20 mg/mL) (F-FURP) was supplied by Fundação para o Remédio Popular- FURP (São Paulo, Brazil). Povacoat® Type F (polyvinyl alcohol/acrylic acid/methyl methacrylate copolymer, molecular weight 40,000) was donated from Daido Chemical Corporation (Osaka, Japan). D-mannitol (MAN) was purchased from Wako Pure Chemical Industries Company, Ltd. Stabilized zirconia (zirconium oxide) beads with diameters of 0.1 mm were purchased from Retsch Company, Ltd. (Haan, Germany). Ultra-purified water Milli-Q®, Millipore GmbH (Millipore, Darmstadt, DE) was used for all formulations. The water conductivity used for ZP analysis was 60 μS/cm. The other chemicals were of analytical reagent grade. The *Mycobacterium tuberculosis* (strain ATCC 25618/H37Rv) and HepG2 cells were donated from the Laboratory of Molecular Biology Microbiology for the Diagnosis by Professor Ph.D. Mario Hiroyuki Hirata (São Paulo, Brazil).

2.2. Preparation of Rif nanosuspension by miniaturized wet-bead milling method using Box-Behnken Design (BBD)

Rif nanosuspensions were prepared by miniaturized wet-bead milling method. The formulations contained 3 to 5% (w/w) Rif, 10 to 20% (w/w) of zirconia beads (ZIR) (0.1 mm) and 1 to 3% (w/w) POVA aqueous solution for total weight of 10 g. The milling chamber consisted of a 20-mL glass vial. The final set was composed of two magnetic stir bars, cross-shaped (20 × 20 mm) (Max Labor, Brazil) arranged vertically stacked on top of each other (Fig. 1). For each formulation, first, the amount of RIF and ZIR was transferred to the vial; then, the POVA aqueous solution and, finally, the magnetic stir bars. The vials were stirred in an Ika® RTC basic magnetic stirrer plate (Ika, Germany) at 800 rpm (speed of stirring) for 3 days at 25 °C. The nanosuspensions obtained were removed using a pipette after precipitation of zirconia beads as a result of their high density (3.7 g/cm^3).

2.2.1. Box-Behnken Design (BBD)

Box-Behnken statistical design with three factors, three levels, and 15 runs was applied to understand the impact of the independent variables under controlled conditions (Section 2.2). The independent and dependent variables are listed in Table 1. The polynomial Equation 1 (Eq. (1)) generated by this experimental design Minitab® 18 (Minitab Inc., State College, PA, US) and Statistica™ 13 (Statsoft Inc., OK, US) was as follows:

$$Y_i = a_0 + a_1 X_1 + a_2 X_2 + a_3 X_3 + a_{12} X_1 X_2 + a_{13} X_1 X_3 + a_{23} X_2 X_3 + a_{11} X_1^2 + a_{22} X_2^2 + a_{33} X_3^2 \quad (1)$$

where *Yi* (HD = Hydrodynamic diameter) is the dependent variable; a_0 is the intercept; a_1 to a_{33} are the regression coefficients; and X_1 (Rif), X_2 (ZIR) and X_3 (POVA) are the independent variables.

2.2.2. Optimization of Rif nanosuspension

The derived polynomial equation was verified using a checkpoint analysis. Values of independent variables were taken at two points, which generated two formulas (F1-Rif and F2-Rif nanosuspensions). The theoretical values (predicted HD), calculated by substituting the values in the polynomial equation, were compared with the experimental values (observed HD).

2.3. Particle size, zeta potential and morphology characterization

2.3.1. Laser diffraction

The larger particles or aggregates (> 3 to 5 mm) and size distribution were investigated by laser diffractometry (LD) using a Granulometer Cilas 1900 (Cilas, Orléans, FR). The samples were analyzed using the Fraunhofer theory. The dispersing medium was Rif saturated solution. The results were expressed by the volume-weighted diameters d(v;0.1), d(v;0.5), and d(v;0.9). These values represent the percentage of particles below a given size (nm).

2.3.2. Dynamic light scattering (DLS)

The HD of the Rif nanocrystals was determined by DLS, using a Zetasizer Nano ZS 90 (Malvern Instruments Ltd., Malvern, UK) at 25 °C and 90° (n = 10). Also, the polydispersity index (PdI) was determined as a measure of the width of the size distribution. The samples were previously diluted in Rif saturated solution at suitable concentrations.

2.3.3. Zeta potential (ZP) determination

The ZP was determined using Zetasizer Nano ZS (Malvern Instruments Ltd., Malvern, UK) by laser Doppler electrophoresis method. The field strength applied was 20 V/cm. The electrophoretic mobility (EM) was converted to the ZP in mV using the Helmholtz–Smoluchowski equation. ZP measurements were carried out in Rif saturated solution with a conductivity adjusted to 60 μS·cm^{-1} by adding NaCl 0.9% (w/v), to avoid ZP fluctuations caused by the difference in conductivity (n = 3).

2.3.4. Scanning electron microscopy (SEM) and transmission electron microscopy (TEM)

Rif raw material was analyzed using a SU-1500 scanning electron microscope (SEM) (Hitachi High-Technologies, Tokyo, JP). Samples were measured using 15 kV acceleration voltage. The particle size and morphology of Rif raw material and Rif nanocrystals were evaluated using a transmission electron microscopy JEOL JEM-1010 (Jeol, Tokyo, Japan). The size particle was determined by Imagen.j® software (National Institutes of Health, Bethesda, MD, US). The samples were diluted in Rif saturated solution. Observations were made at an excitation voltage of 80 kV and performed at magnifications of 25,000×–40,000×.

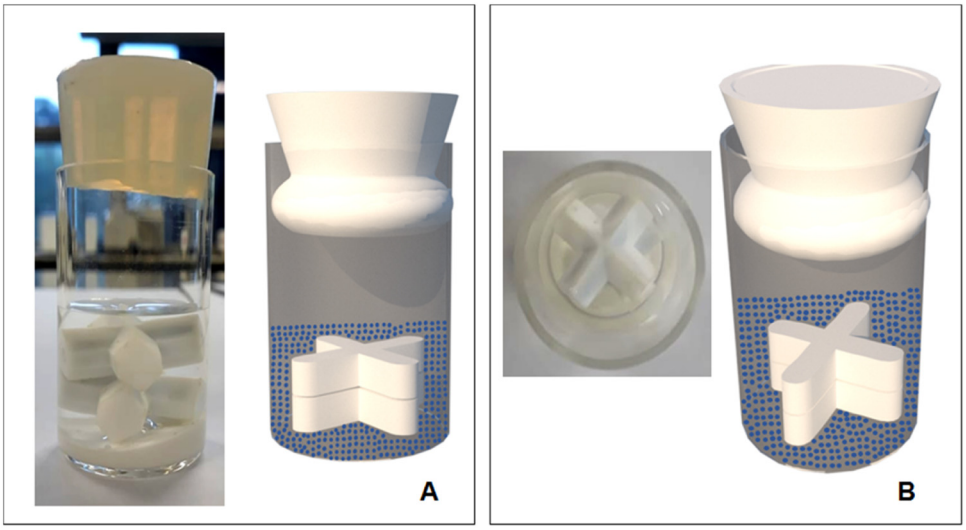

Fig. 1. Scheme of miniaturized wet-bead milling method A: Front view and B: Top view.

Table 1
Variables and levels in Box-Behnken Design to prepare Rif nanocrystals.

Independent variables (%w/w)	Levels		
	Low (−1)	Medium (0)	High (+1)
Rif (X_1)	3.00	4.00	5.00
ZIR (X_2)	10.00	15.00	20.00
POVA (X_3)	1.00	2.00	3.00
Dependent variable			
HD: Hydrodynamic diameter (z-average) of the nanocrystals			

Rif: Rifampicin; ZIR: Zirconia beads; POVA: Povacoat®.

2.4. Characterization of physical state

2.4.1. Differential scanning calorimetry (DSC)

DSC analyses were performed using DSC 7020 (Exstar, Bunkyo-Ku, JP) each sample was carefully weighed, transferred to aluminum crucibles, sealed and submitted to temperature from 25 °C to 350 °C at a scanning rate of 10 °C/min of a dynamic atmosphere of the nitrogen with the empty 50 mL·min^{-1}.

2.4.2. Powder X-ray diffraction (PXRD)

XRD patterns were obtained using Bruker Diffractometer Model D8 Advance Da Vinci (Bruker, Japan), with Cu- Kα radiation generated at 40 mA and 40 kV.

2.5. Nanosuspension lyophilization

The lyophilization procedure was performed in TDS-00209-A (FTS Systems, Stone Ridge, NY, US). The nanosuspensions samples were frozen at −40 °C before primary and secondary drying steps. After freezing, primary drying was started at −30 °C at a pressure of 100 mTorr. Finally, secondary drying was done at temperatures of 10 °C for 300 min and 100 mTorr of pressures. Mannitol 5% (w/v) was used as cryoprotectant. After the lyophilization, the Rif nanocrystals were re-suspended in the same volume of water of the original formulations.

2.6. Saturation solubility measurement

Solubility studies were performed using the shake-flask method in a shaker Tecnal TE 4080 (Tecnal, Sao Paulo, Brazil). An excess of the sample of Rif nanocrystals (F1-Rif and F2-Rif lyophilized nanosuspensions) and Rif raw material were added in lab jars containing 10 mL of purified water (pH 6.5), acetate buffer pH 4.5 and phosphate buffer pH 6.8 and 7.2, prepared according to the American Pharmacopeia [22]. The samples were transferred to the shaker at 37 °C for 72 h. After this time, an aliquot from each sample was withdrawn and filtered through a 0.45 μm pore-size membrane. The content of rifampicin was determined using Evolution 201 UV–VIS spectrophotometer (Thermo Scientific, São Paulo, Brazil) at 472 nm. Analysis of variance (ANOVA) with a post-hoc Tukey test was performed to evaluate the significance of the media in the saturation solubility test using software Minitab® 18 (Minitab Inc., State College, PA, US).

2.7. Determination of rifampicin content, viscosity and pH

The analytical method was developed and validated using Evolution 201 UV–VIS spectrophotometer (Thermo Scientific, São Paulo, Brazil). Accurately weighed 0.15 mg of Rif nanosuspensions and micronized rifampicin commercial suspension (20 mg/mL) were dissolved in 30 mL of ethanol by ultrasonic method. Then the volume was completed to 50 mL with water. Finally, the samples were filtered with a 0.45 μm membrane before analysis by spectrophotometry at 472 nm.

The viscosity was performed using a digital viscometer Brookfield model DV-I Prime (AMETEK Brookfield, MA, US) at room temperature (25 °C) (n = 3). The final pH of the formulations was measured via a Mettler Toledo pHmeter (Model InLab ® 73× Series, Ohio, US) at room temperature (25 °C) (n = 3).

2.8. Dissolution test

Dissolution test of Rif nanosuspensions and micronized rifampicin commercial suspension (20 mg/mL) (F-FURP) was carried out for 60 min in 900 mL of phosphate buffer solution (pH 6.8) with constant stirring at 50 rpm in a dissolution apparatus 2, 708-DS Dissolution Apparatus (Agilent Technologies, Santa Clara, CA, US) at 37 °C. The amount of sample for the test was adjusted to obtain 200 mg of Rif. Finally, the amount of dissolved Rif was determined by spectrophotometric method at 472 nm.

2.9. Stability studies

The stability study for Rif nanosuspensions was evaluated at 4 °C for two years. HD and PdI value measurements were performed using

Zetasizer Nano ZS (Malvern Instruments Ltd., Malvern, UK) in triplicate (n = 3).

2.10. Minimal inhibitory concentration (MIC) by broth dilution method

The metabolic activity of *Mycobacterium tuberculosis* H37Rv was determined by colorimetric MTT [23]. The MIC was performed in a biosafety cabinet type BSC Class II A using biosafety level 3 practices in the mycobacteriology laboratory. The strain ATCC 25618/H37Rv was obtained from the American Type Culture Collection (ATCC) and maintained at Laboratory of Microbiology. The activity of the organism was determined by colorimetric MTT (3-(4, 5-dimethylthiazolyl-2)-2, 5-diphenyltetrazolium bromide) reduction assay in 96-well plates (Falcon 3072, BD, Argentina). The microbial suspension was transferred using a multichannel pipette, in each well of a 96-well plate at 10^6 CFU/well (50 μL), and *N*-acetylcysteine (NAC) (50 μL) diluted in Middlebrook 7H9 broth medium with 10% (w/v) oleic acid albumin dextrose complex (OADC) added at the indicated concentrations. The plates were incubated at 37 °C in air containing 5% CO_2, for 5 days. After this period, the samples of Rif nanosuspensions (F1-Rif and F2-Rif), micronized rifampicin commercial suspension (20 mg/mL) (F-FURP) and standard rifampicin powder (S-Rif) (Sigma Chemical, St Louis, MO, US) diluted to concentrations at 8.0, 4.0, 2.0, 1.0, 0.5, 0.25, 0.125 and 0.063 μg/mL were transferred to the cells. The assay was incubated for 48 h at 37 °C, in air containing 5% CO_2. Then, the MTT salt was added to each well-plate and incubated for 3 h. Finally, an aliquot of 100 μL of lysis buffer (20% w/v of sodium dodecyl sulfate and 50% of dimethylformamide in distilled water) was added, and the cultures were incubated overnight at 37 °C in 5% CO_2. Bacterial cultures treated with standard rifampicin powder (1.0 μg/mL) were used as a positive control for growth inhibition and with only Middlebrook 7H9 broth medium as the negative control. The MIC was defined as the concentration at which no microbial growth was observed visually or spectrophotometrically via readings of optical density (OD) at 570 nm (TECAN Safire 2, Mannedorf, Switzerland). The means of the values of absorbance (n = 24) for the F1-Rif, F2-Rif, F-FURP, and S-Rif were compared using ANOVA. The magnitude of the differences observed in the ANOVA was revealed using a multiple comparison test, the Tukey test.

2.11. In vitro cytotoxicity studies

The MTT assay determined the cytotoxic effect of Rif nanosuspensions on HepG2 cells. These cells were cultured in 96-well plates at a concentration of 1×10^5 cells/well, and incubated at 37 °C, in a 5% CO_2 incubator. After 24 h, the culture supernatant was changed, and different amounts of Rif were added to produce final concentrations of 1.0, 5.0, 10.0, 15.0, 25.0, and 75.0 μg/mL in Middlebrook 7H9 broth medium. Also, Middlebrook 7H9 broth medium with Dimethyl sulfoxide (DMSO) 5.0% (w/v) was added as positive control (total cell death) and only Middlebrook 7H9 broth medium as the negative control (100% cell viability). The plates were incubated for 24 h. Then, 20 μL of MTT (methyl-tetrazolium [3-(4,5-dimethylthiazol-2-yl)-2,5-diphenyltetrazolium bromide]) (Sigma-Aldrich, US) at a concentration of 5.0 mg/mL was added to each well. The plates were incubated for 3 h at 37 °C in a 5% CO_2 incubator. The growth medium was removed; 200 μL of DMSO and 20 μL of glycine buffer were added and incubated at room temperature for 30 min. The appearance of purple color demonstrated the presence of viable cells due to the formation of formazan crystals. The absorbance was determined at 570 nm using Microplate reader Biotek-PowerWave XS2 (BioTek Instruments, Inc., Winooski, VT, US). Percent of growth inhibition was determined using the following equation:

$$\text{Growth inhibition (\%)} = [(C - T)/C] \times 100$$

where C is the mean absorbance of the control group, and T is the mean absorbance of the test group.

This method is recommended and standardized according to ISO 10993-5:2009 Biological evaluation of medical devices - Part 5: Tests for in vitro cytotoxicity [24].

3. Results and discussion

3.1. Preparation of Rif nanosuspensions by miniaturized wet-bead milling method using Box-Behnken Design (BBD)

Rif nanosuspensions were prepared by miniaturized wet-bead milling method (Section 2.2). After three days, the particle size was reduced to about to 500 nm compared to the initial size of 50 μm, a 100-fold decrease in the size. This small-scale approach, being simple and low-cost, allows for screening of drug and stabilizer concentrations, and identifies critical process parameters [15].

3.1.1. Box-Behnken Design (BBD)

The Box-Behnken design was used to evaluate the effects of the independent variables on the dependent variable, hydrodynamic diameter. BBD requires fewer experiments (15 formulas) compared to a full factorial design (27 formulas), maintaining a similar statistical power level. The BBD design, HD, and PdI results are shown in Table 2.

The Supplemental Table S1 presents the analysis of variance (ANOVA) for HD. The p-values < 0.05 ($\alpha = 0.05$) showed the significance of each main effect and their interaction. The lack-of-fit showed p-value equal to 0.484, which indicated the fitness of the selected model. In this study, the regression analysis revealed coefficient of determination (R^2) of 99.76%, adjusted R^2 (adj-R^2) of 99.32%, and predicted R^2 (pred-R^2) of 97.31% (Supplemental Table S1). When these values differ significantly, it is an indication that nonsignificant terms were included in the model [25]. For the developed model, the three R^2 values were close, which indicates that the model was representative of the data, and the variables were representative, regarding HD.

Fig. 2 shows the optimized condition to decrease the HD to values < 348 nm: Rif concentration < 3.5% (%w/w); concentration of POVA aqueous solution in the range of 2.4 to 3.2% (%w/w) and 14 to 20% (%w/w) of ZIR. The reduction of particle size is a result of the collisions produced between the particles of the drug substance with itself and with the grinding beads in the grinding chamber [26–28]. The Rif concentration in the system allowed an effective mechanical collision and shear forces [27]. The study showed that POVA concentration is critical and can affect the milling results. High polymer concentration may slow down the movement of zirconia beads, hinder the energy delivery, delay production, and jellify the nanosuspension during

Table 2
Box-Behnken experimental design and observed responses.

Formula	Rif	ZIR	POVA	HD + SD (nm)	PdI
	(%w/w)				
1	3.0	10.0	2.0	407.2 ± 4.5	0.1
2	5.0	10.0	2.0	393.3 ± 1.0	0.2
3	3.0	20.0	2.0	362.9 ± 4.3	0.2
4	5.0	20.0	2.0	390.9 ± 2.8	0.1
5	3.0	15.0	1.0	401.6 ± 0.3	0.2
6	5.0	15.0	1.0	377.9 ± 6.9	0.2
7	3.0	15.0	3.0	336.6 ± 1.6	0.2
8	5.0	15.0	3.0	362.9 ± 5.5	0.3
9	4.0	10.0	1.0	421.8 ± 4.0	0.1
10	4.0	20.0	1.0	442.4 ± 8.9	0.2
11	4.0	10.0	3.0	428.8 ± 5.3	0.2
12	4.0	20.0	3.0	355.3 ± 2.6	0.2
13	4.0	15.0	2.0	356.4 ± 4.5	0.2
14	4.0	15.0	2.0	360.4 ± 2.1	0.2
15	4.0	15.0	2.0	360.8 ± 3.7	0.2

Rif: rifampicin; ZIR: zirconia beads; POVA: Povacoat®, HD: hydrodynamic diameter, SD: standard deviation, PdI: polydispersity index.

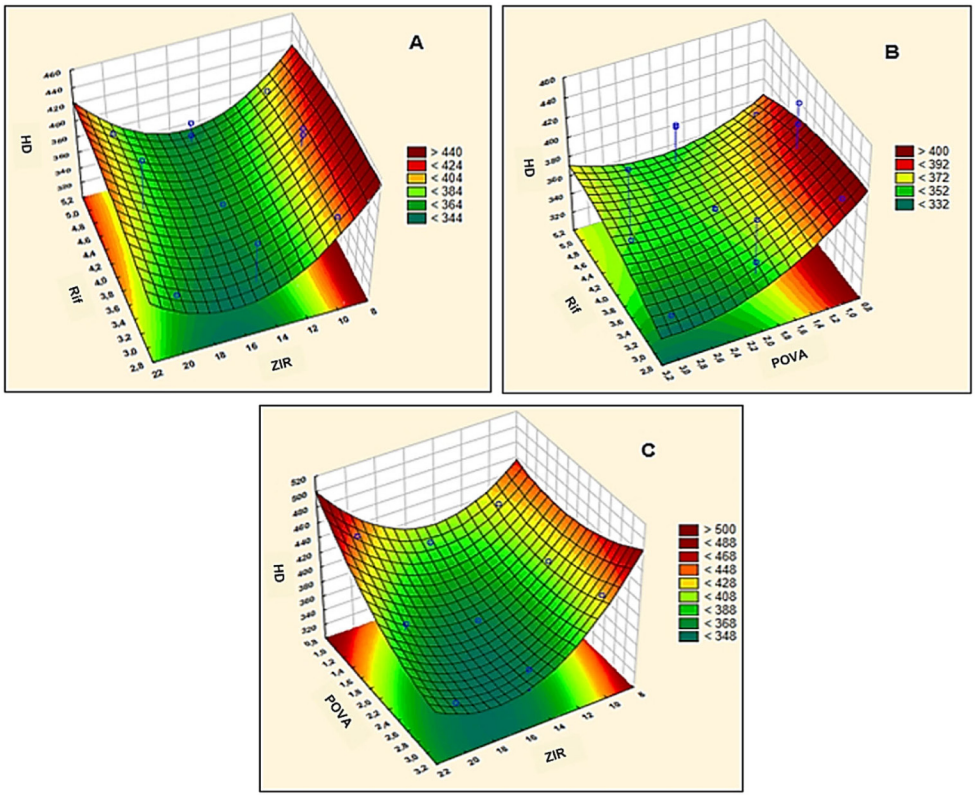

Fig. 2. Three-dimensional response surface plot showing the effects of the mutual interactions between two independent variables on the HD of the Rif nanocrystals. A: Rif and ZIR (POVA 2.0%w/w), B: Rif and POVA (ZIR 15.0%w/w) and C: POVA and ZIR (Rif 4.0%w/w).

production [29,30]. A larger number of zirconia beads with high density are beneficial for obtaining fine particles [27,28].

A second-order polynomial equation for HD (dependent variable) was generated, Eq. (2).

$$\begin{aligned} HD\ (nm) = {} & 799.90 - 2.50\ Rif - 44.48\ ZIR - 67.54\ POVA - 6.48\ Rif \\ & * Rif + 1.43\ ZIR * ZIR + 17.03\ POVA * POVA + 2.09\ Rif \\ & * ZIR + 12.50\ Rif * POVA - 4.70\ ZIR{*}POVA \end{aligned} \quad (2)$$

3.1.2. Optimization of Rif nanosuspension

For the mathematical model verification, it was found that the observed and predicted HD values of F1-Rif and F2-Rif (Fig. 3) were similar (Table 3) and presented monomodal distribution (Supplemental Fig. S1). Thus, the obtained mathematical model was valid for predicting the HD.

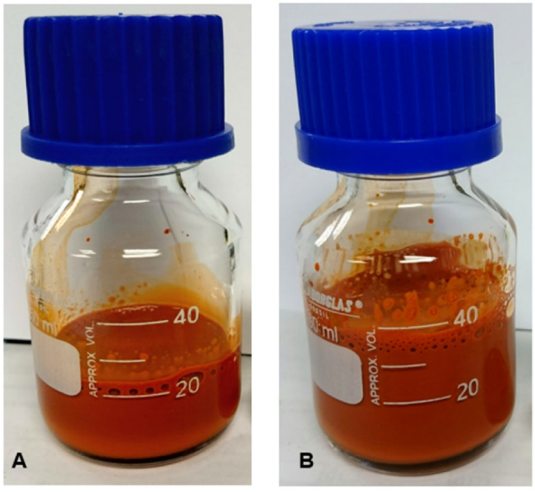

Fig. 3. Rif nanosuspensions obtained by miniaturized wet-bead milling method. A: F1-Rif and B: F2-Rif.

Table 3
Observed and predicted hydrodynamic diameter (HD) by dynamic light scattering (DLS) for optimized Rif nanosuspension (F1-Rif and F2-Rif) (n = 3).

Sample	Rif	ZIR	POV	HD (nm)		95% CI
	(%w/w)			Predicted	Observed	
F1-Rif	3.25	20.00	2.57	345.10	340.60 ± 5.40	339.70; 350.30
F2-Rif	3.28	20.00	2.00	370.10	364.20 ± 4.50	365.30; 374.80

Rif: rifampicin; ZIR: zirconia beads; POVA: Povacoat®, CI: confidence interval.

3.2. Particle size and morphology characterization

The Rif raw material had around 50 μm in diameter. Tables 3 and 4 show Rif nanocrystal particle sizes in the nanoscale range. Due to increased saturation solubility, Rif nanocrystals can dissolve during the

Table 4
Mean particle diameters of Rif raw material, F1-Rif and F2-Rif by laser diffraction (LD) (n = 10).

Samples	d (v; 0.1) (μm)	d(v; 0.5) (μm)	d(v; 0.9) (μm)	MD (μm)
Rif	35.2 ± 0.1	48.9 ± 0.1	66.8 ± 0.1	50.1 ± 0.1
F1-Rif	0.4 ± 0.1	0.6 ± 0.1	0.9 ± 0.1	0.6 ± 0.1
F2-Rif	0.1 ± 0.1	0.6 ± 0.1	1.7 ± 0.1	0.8 ± 0.1

LINK Excel.SheetBinaryMacroEnabled.12 "C:\\Users\\Katherine\\AppData\\Roaming\\Microsoft\\Excel\\Libro1 (version 1).xlsb" "Hoja1!F8C6:F14C10" \a \f 4 \h * MERGEFORMAT d(v;0.1), d(v;0.5), and d(v;0.9): volume-weighted diameters, MD: mean diameter.

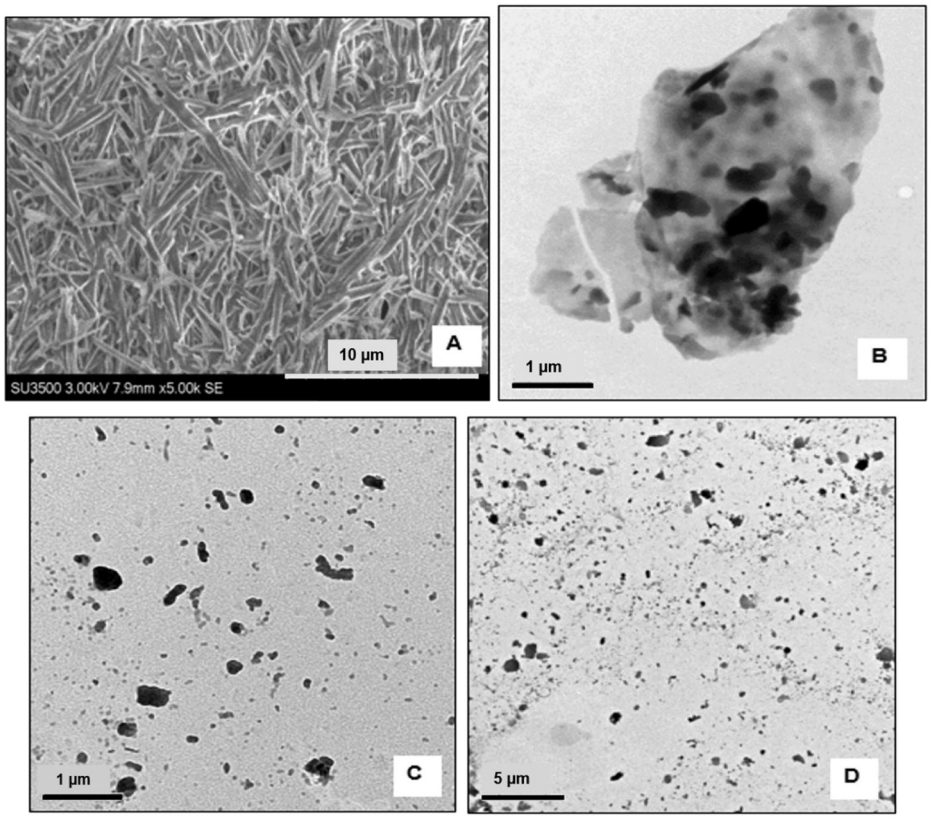

Fig. 4. SEM micrograph: (A) Rif raw material (magnification 5000×). TEM micrographs: (B) Rif raw material (magnification 25,000×), (C) F1-Rif nanocrystals (magnification 25,000×) and (D) F2-Rif nanocrystals (magnification 5000×).

measurements causing differences in size and polydispersity index (PdI). The Rif saturated solution was used to address this problem [10,31]. The similar results of particle size using different techniques (DLS and LD) (Tables 3 and 4) indicated an adequate performance of miniaturized wet-bead milling method.

The SEM micrograph (Fig. 4A) of RIf raw material showed microparticles with typical needle morphology of the crystals. Fig. 4B (TEM micrograph) revealed the tendency of Rif particles to form aggregates from smaller particles. This feature is a challenge in product development, which requires the proper choice of the stabilizing agent aiming to achieve adequate stability to the system. TEM micrographs of nanocrystals (Fig. 4C–D) showed their semi-spherical morphology and absence of aggregates. The particle size was drastically decreased from microscale to nanoscale. The results showed particle sizes between 40 nm to 500 nm in the nanosuspensions. Similar results were found by the measurements based on DLS and LD methods [32,33].

3.3. Nanosuspension lyophilization

The addition of excipients (cryoprotectants and lyoprotectants) in the formulations is necessary to avoid changes in the nanocrystals. The characteristics of an excellent freeze-dried product include an intact cake. This cake, when redispersed has to occupy the same volume as the original frozen dough (Fig. 5) [34]. Mannitol was used successfully as cryoprotectant at a concentration of 5% (w/v) to avoid the aggregation of drug nanocrystals. This sugar is used since it recrystallizes around the nanocrystals during the water-removal operation and prevents the particle interaction and the formation of aggregate [35,36]. After the lyophilization, the Rif nanocrystals redispersion time was rapid and without observation of apparent aggregates. Table 5 shows the results of HD, PdI, and ZP. These parameters were unaffected by the freeze-drying process. Additionally, TEM micrographs (Fig. 6) show the semi-spherical morphology without aggregates remaining.

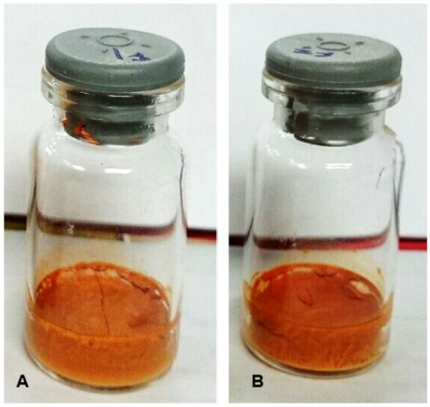

Fig. 5. Rif nanosuspension lyophilized A: F1-Rif and B: F2-Rif.

3.4. Characterization of physical state

The Cambridge Structural Database (CSD) provides seven crystalline forms of rifampicin [5] with two polymorphic forms having been identified through thermal analysis [37]. The DSC study confirmed that the rifampicin used was polymorphic form II with a melting peak at 192.3 °C, immediately followed by recrystallization to form I (exotherm at 200 °C). This feature is a characteristic of a solid-liquid-solid transition. The drug finally decomposed above 248.9 °C (Fig. 7) [38]. Fig. 7, DSC curve, demonstrated rifampicin raw material and lyophilized rifampicin nanocrystals presented polymorph form II. The only difference observed was a shift in temperature of thermic events by the reduction of particle size or the presence of the stabilizer [39,40]. The DSC curve of physical mixture presented a sum of the thermal events of rifampicin and Povacoat® and was similar to the curves of nanocrystal

Table 5
Hydrodynamic diameter (HD), polydispersity index (PdI) and zeta potential (ZP) of F1-Rif, F2-Rif and redispersed rifampicin nanocrystals in water (n = 3).

Samples	Before lyophilization			After lyophilization (redispersed nanocrystals)		
	HD (d. nm)	PdI	ZP (mV)	HD (d. nm)	PdI	ZP (mV)
F1-Rif	340.6 ± 5.4	0.2 ± 0.1	−8.8 ± 0.4	345.7 ± 3.4	0.3 ± 0.1	−9.0 ± 0.4
F2-Rif	364.2 ± 4.5	0.3 ± 0.1	−9.0 ± 0.1	363.2 ± 2.9	0.2 ± 0.1	−9.0 ± 0.1

formulations. These results confirmed that the crystalline characteristic of the drug substance was maintained after the nanonization process and demonstrated the lack of interactions between the drug and excipients [41].

The polymorphic form II of rifampicin raw material is distinguishable by its XRD pattern (XRD-p) with characteristic diffraction peaks exhibited at 9.93 and 11.10° 2θ (Fig. 8) [38]. Povacoat® was reported as a semicrystalline polymer with a prominent diffraction peak at 19.2° 2θ [18]. The XRD-p of mannitol (MAN) determined the presence of form III of D-mannitol [42]. The XRD-p of the lyophilized Rif nanocrystals (F1-Rif and F2-Rif) showed the combined peaks of the pure components (Rif, POVA, and MAN) as well as the presence of the peaks 9.93 and 11.10° 2θ of polymorphic form II of Rif. The less intense peaks were due to the presence of 3.25 (%w/w) or 3.28 (%w/w) Rif in the nanosuspensions and the significant reduction in the particle size induced by the milling process. Also, these peaks are a result of the dilution of the particles with the stabilizer (POVA) and cryoprotectant (MAN) [21,43]. Similar results were observed in the crystallinity of griseofulvin after nanonization. The XRD-p of MAN proved to be so strong that it was difficult to check the crystallinity of the milled griseofulvin [20]. Finally, as a conclusion of the results of DSC and XRD-p evaluation, the crystalline state of Rif was not influenced by the miniaturized wet-milling process.

3.5. Determination of rifampicin content, viscosity and pH

The Rif content for F1-Rif and F2-Rif was 96.3% and 96.0% (w/v), respectively, which was higher than the micronized rifampicin commercial suspension (20 mg/mL) (Table 6). The lower drug content found (88.9%) was due to its high viscosity (725.9 cP), which makes sample homogenization problematic. In contrast, nanosuspensions offer the possibility of incorporating a high concentration of the drug substance into a reduced volume of the dispersion medium, while obtaining products with lower viscosity (F1-Rif and F2-Rif, both 3.1 cP) compared to the commercial product. Therefore, the administration of the nanosuspension could reduce the dose by half, which might improve the long-term treatment for the elderly and children by reduce side effects [44–46].

The pH is an important parameter to avoid RIF degradation. Table 6 shows the pH for F1-Rif and F2-Rif formulations was 6.55 and 6.60, respectively. Rifampicin is most stable in the range of pH 5 to 7 (pKa values of 1.7 and 7.9) [47,48]. However, in an acidic medium, rifampicin hydrolyzes and forms degradation products such as 1-amino-4-methyl piperazine [47,49]. For this reason, solid preparation is more appropriate. The lyophilization process was used to provide a solid formulation. This approach increases its chemical stability and reduces the possible hydrolysis process of rifampicin in aqueous medium.

3.6. Saturation solubility

Fig. 9 shows the results of the saturation solubility of Rif raw material (Rif) and Rif nanocrystals (F1-Rif and F2-Rif). The analysis of variance (ANOVA) (Supplemental Table S2) revealed a significant difference between the solubility means among the Rif nanocrystals and Rif raw material (p-value equal to and < 0.001; $\alpha = 0.05$).

Subsequently, the Tukey test (Table 7) revealed the AB pH 4.5, water and PB pH 7.2 media presented significant differences in saturation solubility of F1-Rif and F2-Rif compared to Rif raw material. Additionally, in PB pH 6.8 medium, the three samples showed significant differences. Thus, this medium was chosen as the dissolution test medium since it is more discriminative. These results confirm the increased saturation solubility of Rif nanocrystals.

The size reduction increased the solubility of the two formulations (F1-Rif and F2-Rif) in all media. The Rif nanocrystals increased solubility up to 1.74-fold in water compared with the raw drug substance. Agrawal and collaborators found that Rif bioavailability is variable due to a limited dissolution rate in the acidic medium. Immediate release (IR) formulations might disintegrate in the stomach but might not release the drug rapidly for optimum bioavailability [38]. The results showed a higher saturation solubility occurred at acid pH (acetate buffer pH 4.5), where rifampicin exhibits usually lower solubility. The Noyes–Whitney Kelvin and Ostwald–Freundlich equations establish

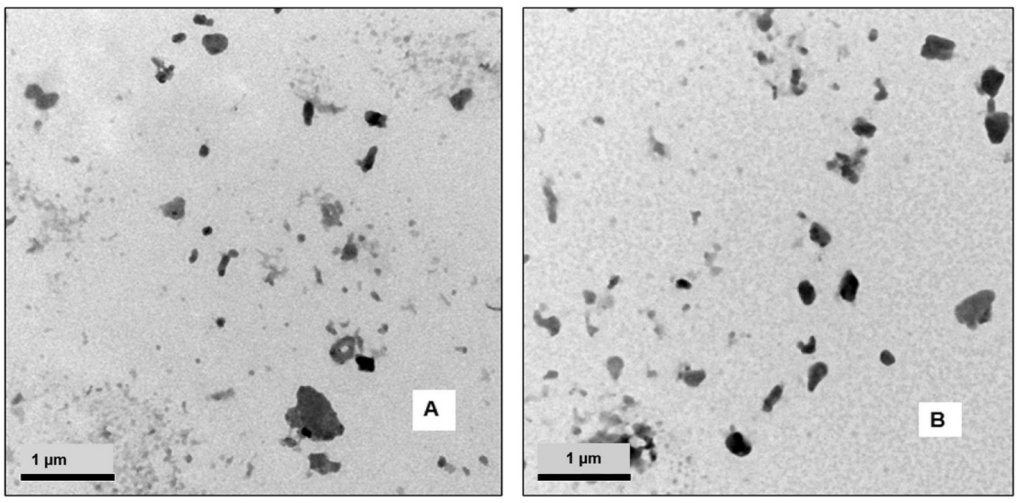

Fig. 6. TEM micrographs (A) F1-Rif (magnification 25,000×) and (B) F2-Rif (magnification 25,000×) lyophilized after redispersion.

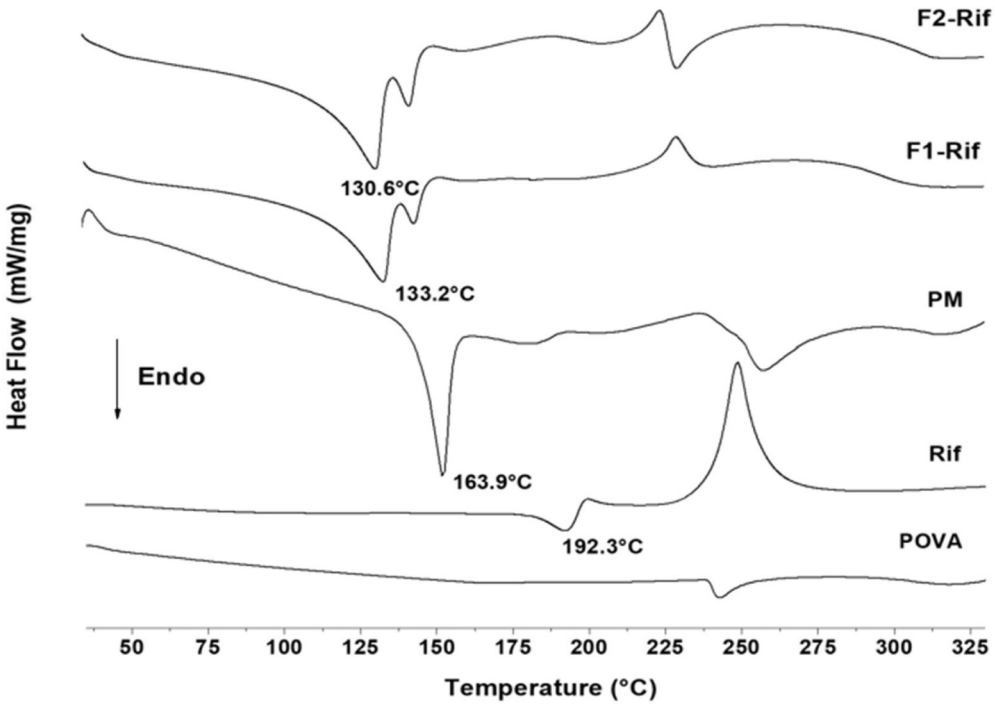

Fig. 7. DSC curves of rifampicin raw material (Rif), Povacoat® (POVA), physical mixture (PM) and lyophilized rifampicin nanocrystals (F1-Rif and F2-Rif).

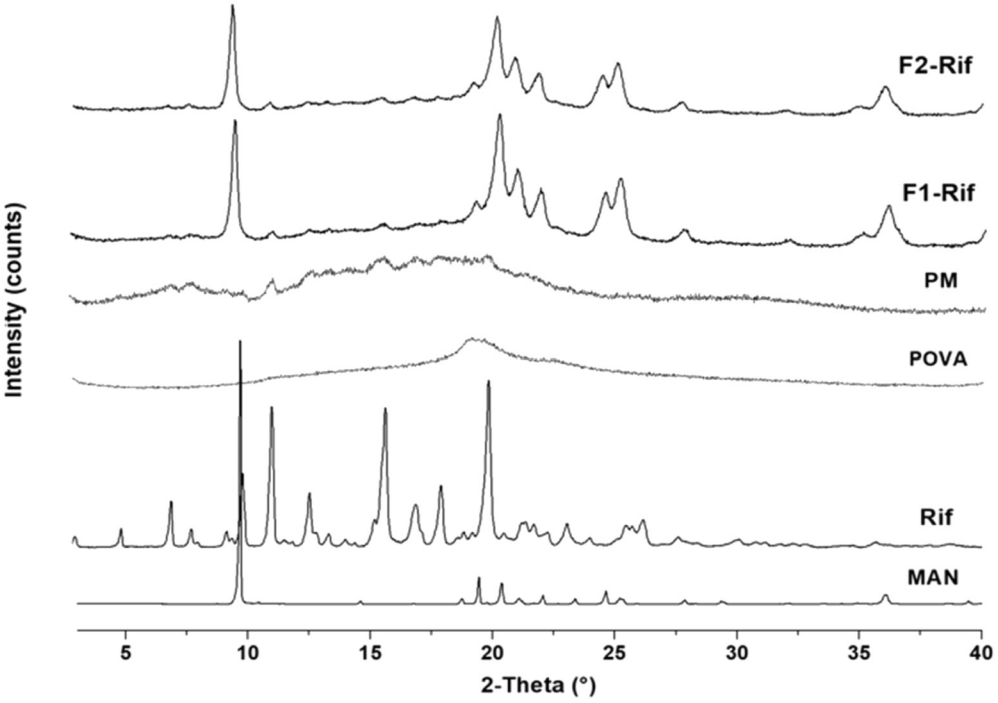

Fig. 8. Powder X-ray diffractograms of rifampicin raw material (Rif), Povacoat® (POVA), mannitol (MAN), physical mixture (PM), and lyophilized Rif nanocrystal (F1-Rif and F2-Rif).

that the reduction of the particle size increases surface area allows for higher interaction with dissolution media (biological fluids). Thus, it promotes a high dissolution rate [42,50–54]. The increase of the saturation solubility and the adhesion to biological membranes of drug nanocrystals allow an increase in the concentration gradient and subsequently permeation of the drug through gut membranes [55–58]. Frequently, variability in oral absorption is common for class II drugs in fed vs. fasted state. Due to their in vivo properties nanocrystals can reduce fasted and fed state variability [58–60].

3.7. Dissolution test

The dissolution rate and saturation solubility are essential factors affecting oral absorption, which can be improved by a reduction in particle size [61,62]. The dissolution profiles for F1-Rif, F2-Rif, and micronized rifampicin commercial suspension (20 mg/mL) (F-FURP) are shown in Fig. 10. Rif nanosuspensions showed the highest dissolution rate in a few minutes compared to the F-FURP. The effect of Rif particle size is pronounced in determining solubility [63]. The slow

Table 6
Drug content, pH and viscosity in the Rif nanosuspensions (F1-Rif and F2-Rif) and micronized rifampicin commercial suspension (20 mg/mL) (F-FURP) (n = 3).

Samples	Concentration (mg/mL)	% Rif content (w/v)	Viscosity (cP)	pH
F1-Rif	42.9 ± 0.4	96.3 ± 0.4	3.1 ± 0.1	6.55 ± 0.02
F2-Rif	42.4 ± 0.5	96.0 ± 0.5	3.1 ± 0.1	6.60 ± 0.03
F-FURP	17.8 ± 2.1	89.0 ± 2.1	725.9 ± 6.8	4.49 ± 0.02

dissolution of the commercial suspension can be attributed to the high hydrophobicity of rifampicin shown by poor wetting of drug particles and its particle size (50.1 ± 0.1 μm). Additionally, the commercial suspension shows high viscosity (725.87 cP) compared to the nanosuspensions, which did not allow an adequate stirring in the vessel of apparatus 2. The slope of the dissolution profile is different for nanosuspensions in the initial stage (first 30 min). The dissolution rate of rifampicin nanosuspension was maintained at a higher level throughout the experiment when compared to the commercial product. The large effective surface area and higher apparent saturation solubility of Rif nanocrystals enhance the dissolution rate according to the Noyes-Whitney equation [59]. A higher amount of dissolved drugs can enhance the absorption leading to higher drug plasma concentrations. This can potentially avoid the development of multidrug-resistant (MDR-TB), and Rifampicin mono-resistant tuberculosis (RMR-TB) strains of *Mycobacterium tuberculosis* [64,65], which represent a significant challenge to the global control of tuberculosis.

3.8. Stability study

Drug nanocrystals can agglomerate, aggregate, or precipitate during the preparation or storage. Mostly, the aggregation is due to Ostwald ripening phenomenon, where smaller particles are dissolved faster, and free molecules diffuse to the larger drug particles. This enlargement in particle size will decrease the apparent saturation solubility and the dissolution rate [51,59]. The balance between attractive and repulsive forces in aqueous suspensions can be achieved by adding stabilizers (surfactants and polymers) on the particle surfaces, such as Povacoat® (Supplemental Fig. S2), decreasing the Ostwald ripening emergence. This polymer was initially developed as a film-coating agent and wet granulation binder [18]. Povacoat® can form a dense film that operates as moisture, odor, and oxygen barriers in tablets. This film prevents the passing of oxygen, avoiding the deterioration of the coated tablets. Its high water solubility allows easy preparation of Povacoat® solutions for film coating or granulation binder liquid. The use of this polymer in tablet manufacturing also prevents capping and sticking. Due to its characteristics, it can also be used to produce an orally disintegrating tablet.

When used to prepare nanosuspensions, Povacoat® forms a dense hydrophilic layer around hydrophobic particles providing steric hindrance and repulsions between the particles (steric stabilization). This

Table 7
Tukey multiple comparison test for media (n = 3).

Media	Samples	Mean	Grouping		
AB pH 4.5	F1-Rif	45.48	A		
	F2-Rif	44.88	A		
	Rif	35.72		B	
Water	Rif	47.71	A		
	F1-Rif	39.89		B	
	F2-Rif	39.01		B	
PB 6.8	F1-Rif	47.71	A		
	F2-Rif	42.71		B	
	Rif	27.38			C
PB 7.2	F1-Rif	45.48	A		
	F2-Rif	44.88	A		
	Rif	35.72		B	

AB: acetate buffer, PB: phosphate buffer.

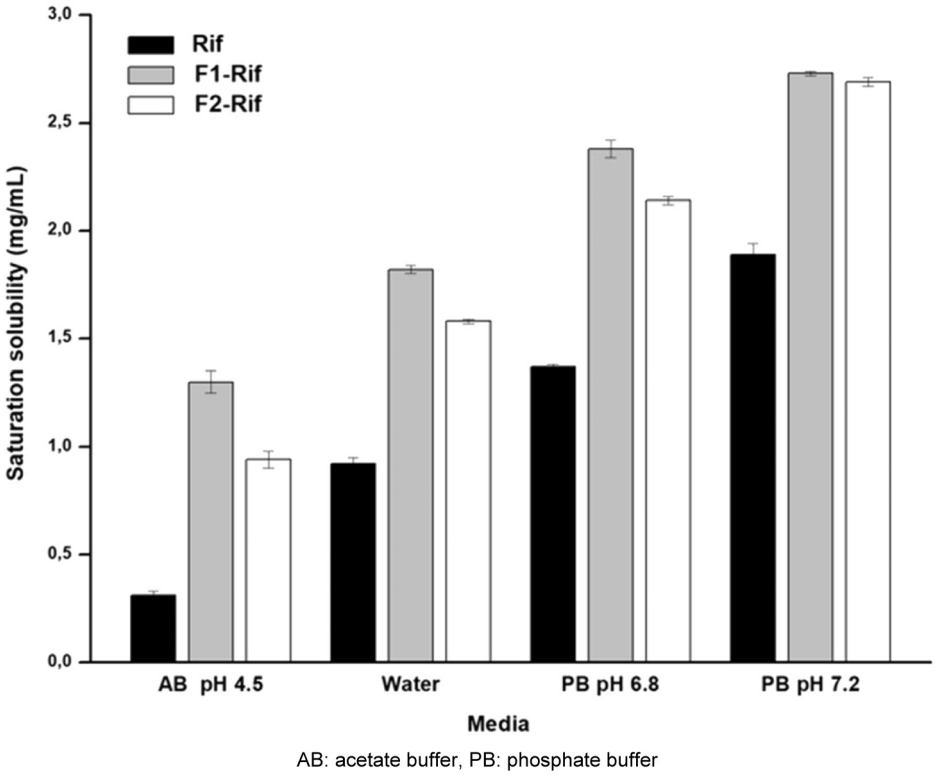

Fig. 9. Solubility (mg/mL) of Rif raw material (Rif) and Rif nanocrystals lyophilized (F1-Rif and F2-Rif) at 37 °C for 72 h (n = 3).
AB: acetate buffer, PB: phosphate buffer.

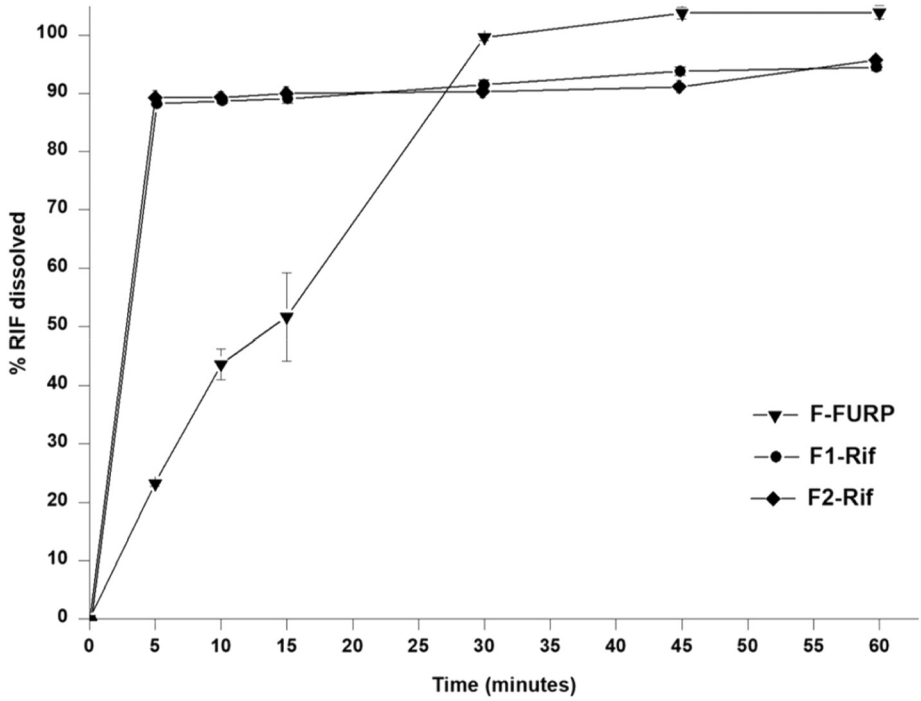

Fig. 10. Dissolution profiles of Rif nanosuspensions (F1-Rif and F2-Rif) and micronized rifampicin commercial suspension (F-FURP) obtained with paddle dissolution test (900 mL of phosphate buffer pH 6.8, 50 rpm, 37 °C) (n = 3).

phenomenon decreases the free energy of the system and interfacial (surface) tension of drug particles, avoiding formation of aggregates due to minimizing the molecular motion of the drug in the dispersed phase [19,20,53,54,66,67]. Povacoat® has demonstrated its potential to prevent the aggregation. This polymer was more efficient than other stabilizers in providing physicochemical stability in the preparation of orotic acid (OA) nanocrystals by a high-energy milling method. The results indicated a notable reduction in the particle size of OA, > 200 times (116 ± 5 nm) when compared with the OA raw material (26.1 μm) [21]. Similarly, Yuminoki et al. obtained griseofulvin (GF) nanocrystals by the same method using polyvinyl alcohol (PVA), hydroxypropyl cellulose (HPC), and polyvinylpyrrolidone (PVP) as stabilizing agents. Drug nanocrystals with Povacoat® showed high dispersion stability, an improvement of solubility and oral absorption compared with the other polymers studied [20].

The stability study is shown in Fig. 11. The particle size of F1-Rif and F2-Rif presented monomodal size distribution with PdI lower than 0.3. No aggregates indicated the physical stability of the system for two years. Homogenous nanosuspensions (PdI < 0.3) can effectively avoid the emergence of the Ostwald ripening phenomenon. The storage temperature was essential to prevent physical instability; higher temperatures can increase the saturation solubility of Rif, the hydrophobic interactions between particles, and the dehydration of polymer [68]. The unchanged particle size for two years proved that Povacoat® was a suitable choice for Rif nanosuspension stabilization.

3.9. Determination of minimum inhibitory concentration (MIC)

The mean absorbance values at 0.25 μg/mL (MIC) (n = 24) for the F1-Rif, F2-Rif, micronized rifampicin commercial suspension (F-FURP) and standard rifampicin powder (S-Rif) are presented in Supplemental Table S3. The analysis of variance (ANOVA) revealed a significant difference between the means among these groups (p-value equal to 0.001; α = 0.05) (Supplemental Table S4).

The Tukey test (Table 8) revealed that the F1-Rif and F-FURP, F2-Rif and S-Rif, F-FURP, and S-Rif did not present significant differences among themselves.

Similar to this study, Schön and colleagues determined that the rifampicin MIC were equal to 0.25 μg/mL and 0.50 μg/mL, respectively, for susceptible *Mycobacterium tuberculosis* H37Rv strain in clinical isolates and for other susceptible *Mycobacterium tuberculosis* [69]. In the present study, the MIC was 0.25 μg/mL; absorbance equal to 0.08075, 0.08713, 0.06756 and 0.07279, respectively for F-FURP, F1-Rif, F2-Rif and S-Rif, indicating that the milling process did not alter the antimicrobial property of the Rif (Supplemental Table S3).

3.10. In vitro cytotoxicity study

For the evaluation of the cytotoxicity, F1-Rif was chosen due to its higher concentration of polymer compared to the F2-Rif. MTT method using HepG2 cells was selected due to the well-known anti-tuberculosis drug-induced liver injury. Cell viability values below 70% characterize significant toxicity of the sample [70,71]. This assay has been used to screen the cytotoxicity of bexarotene nanocrystals and paclitaxel nanoparticles. Bexarotene nanocrystal showed tumorigenic potential reduction in human lung cancer cell line [72]. Similarly, paclitaxel (PTX) nanoparticles were less toxic than pure drug PTX in cancer and resistant cancer cell lines [73]. In the present study, we use hepatocytes to access the in vitro toxicity of Rif nanocrystals.

Table 9 showed that the interaction between rifampicin and the polymer was not cytotoxic. Additionally, no evidence of cytotoxicity was found in any of the tested concentrations since there is no statistically significant difference between the values of cellular viability for these concentrations and those found for the control group. Furthermore, cell viability was > 70% for all concentrations studied, which, according to ISO 10993-5 [24,74], does not have a toxic effect.

4. Conclusion

In this study, a simple miniaturized wet bead milling method demonstrated to adequately reduce the particle size of rifampicin (< 500 nm and 100-fold decrease). The rifampicin nanocrystals showed increased saturation solubility up to 1.74-fold and improved dissolution rate, compared to the commercial product marketed in Brazil. Thus this

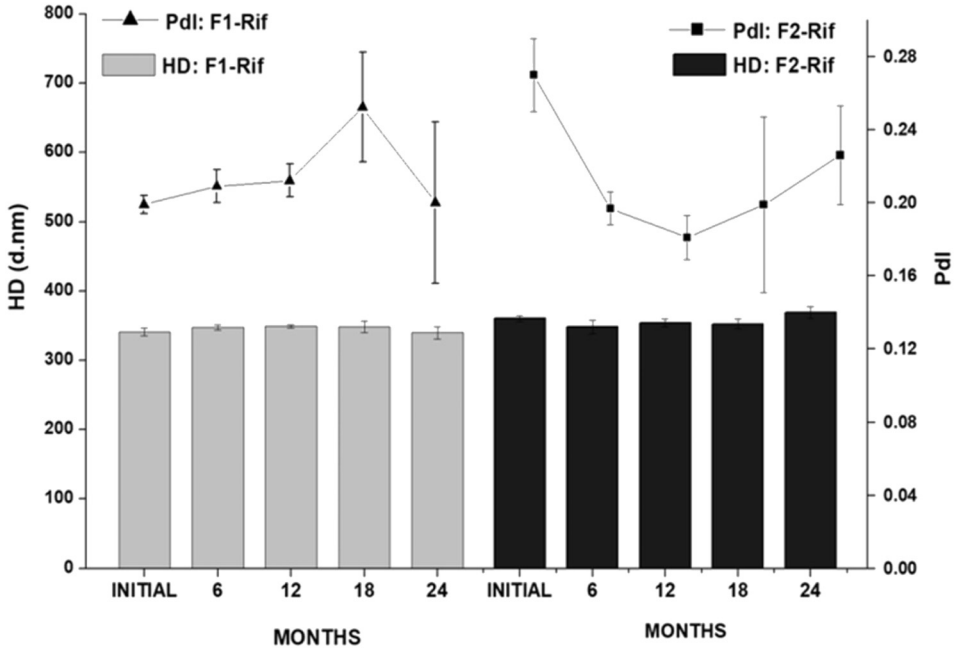

Fig. 11. Hydrodynamic diameter (HD) and PdI of the Rif nanosuspensions (F1-Rif and F2-Rif) stabilized with Povacoat® for 24 months storage at 4 °C temperature (n = 3).

Table 8
Tukey multiple comparison test (n = 24).

Samples	Means	Grouping		
F1-Rif	0.08713	A		
F-FURP	0.08075	A	B	
S-Rif	0.07279		B	C
F2-Rif	0.06756			C

F-FURP: micronized rifampicin commercial suspension, S-Rif: standard rifampicin powder.

Table 9
Absorbance (mean ± SD) and cell viability (%) (n = 6).

Treatments		Abs (570 nm)	% viability
Negative control (DMEM medium)		0.64 ± 0.16	100.00
Positive control (DMSO)		0.02 ± 0.02	3.30
Rifampicin (μg/mL) F1-Rif	1	0.56 ± 0.07	91.30
	5	0.51 ± 0.07	82.20
	10	0.46 ± 0.08	75.10
	15	0.51 ± 0.13	83.00
	25	0.44 ± 0.13	70.70
	75	0.49 ± 0.11	80.40

preparation might increase the oral absorption of this poorly water-soluble drug. Another achievement was that the crystalline state was unchanged after the size reduction and lyophilization. Povacoat® increased the nanosuspension stability up to two years. Furthermore, a 100% increase in drug concentration in the preparations was achieved. F1-Rif and F2-Rif showed antimicrobial properties similar to the commercial product and no evidence of cytotoxicity was observed. These features and a 50% reduction in volume can improve patient adherence throughout the duration of the TB treatment. Thus, rifampin nanosuspensions can provide a platform for developing innovative preparations aiming to combat this disease with improved patient compliance.

Supplementary data to this article can be found online at https://doi.org/10.1016/j.msec.2020.110895.

CRediT authorship contribution statement

Katherine Jasmine Curo Melo: Writing - original draft, Investigation. **Mirla Anali Bazán Henostroza:** Writing - original draft, Investigation. **Raimar Lobenberg:** Supervision. **Nádia Araci Bou-Chacra:** Supervision.

Declaration of competing interest

The authors confirm that there are no known conflicts of interest associated with this publication and there has been no significant financial support for this work that could have influenced its outcome.

Acknowledgment

The authors would like to thank the FAPESP and CAPES Foundation (a federal agency under the Ministry of Education from Brazil-Coordenação de Aperfeiçoamento de Pessoal de Nível Superior) of the Republic of Brazil for financial support of this research work. Academic English Solutions edited the manuscript (https://www.academicenglishsolutions.com).

References

[1] T.M. Daniel, The history of tuberculosis, Respir. Med. 100 (2006) 1862–1870.
[2] World Health Organisation, Global Health TB Report, (2018).
[3] C. Becker, J.B. Dressman, H.E. Junginger, S. Kopp, K.K. Midha, V.P. Shah, S. Stavchansky, D.M. Barends, Biowaiver monographs for immediate release solid oral dosage forms: rifampicin, J. Pharm. Sci. 98 (2009) 2252–2267.
[4] S. Agrawal, R. Panchagnula, Implication of biopharmaceutics and pharmacokinetics of rifampicin in variable bioavailability from solid oral dosage forms, Biopharm. Drug Dispos. 26 (2005) 321–334.
[5] F.H. Allen, IUCr, the Cambridge structural database: a quarter of a million crystal structures and rising, Acta Crystallogr. Sect. B: Struct. Sci. 58 (2002) 380–388.
[6] L. de Pinho Pessoa Nogueira, Y.S. de Oliveira, J. de C. Fonseca, W.S. Costa, F.N. Raffin, J. Ellena, A.P. Ayala, Crystalline structure of the marketed form of rifampicin: a case of conformational and charge transfer polymorphism, J. Mol. Struct. 1155 (2018) 260–266.
[7] P. Liu, X. Rong, J. Laru, B. Van Veen, J. Kiesvaara, J. Hirvonen, T. Laaksonen, L. Peltonen, Nanosuspensions of poorly soluble drugs: preparation and development by wet milling, Int. J. Pharm. 411 (2011) 215–222.
[8] Y. Kawabata, K. Wada, M. Nakatani, S. Yamada, S. Onoue, Formulation design for poorly water-soluble drugs based on biopharmaceutics classification system: basic

approaches and practical applications, Int. J. Pharm. 420 (2011) 1–10.
[9] R. Mauludin, R.H. Müller, C.M. Keck, Development of an oral rutin nanocrystal formulation, Int. J. Pharm. 370 (2009) 202–209.
[10] C.M. Keck, Particle size analysis of nanocrystals: improved analysis method, Int. J. Pharm. 390 (2010) 3–12.
[11] F. Fontana, P. Figueiredo, P. Zhang, J.T. Hirvonen, D. Liu, H.A. Santos, Production of pure drug nanocrystals and nano co-crystals by confinement methods, Adv. Drug Deliv. Rev. 131 (2018) 3–21.
[12] R. Narayan, A. Pednekar, D. Bhuyan, C. Gowda, K.B. Koteshwara, U.Y. Nayak, A top-down technique to improve the solubility and bioavailability of aceclofenac: in vitro and in vivo studies, Int. J. Nanomedicine 12 (2017) 4921–4935.
[13] Liversidge, G.G., Cundy, K.C., Bishop, J., Czekai, D., 1991. Surface modified drug nanoparticles, US Patent, US5145684. (1991).
[14] Kruss, B., Peters, K., Becker, R., Muller, R.H., 1996. Pharmaceutical nanosuspensions for medicament administration as systems with increased saturation solubility and rate of dissolution. Patent US5858410A. (1995).
[15] G.B. Romero, C.M. Keck, R.H. Müller, Simple low-cost miniaturization approach for pharmaceutical nanocrystals production, Int. J. Pharm. 501 (2016) 236–244.
[16] G.B. Romero, A. Arntjen, C.M. Keck, R.H. Müller, Amorphous cyclosporin A nanoparticles for enhanced dermal bioavailability, Int. J. Pharm. 498 (2016) 217–224.
[17] M.L.A.D. Lestari, R.H. Müller, J.P. Möschwitzer, The scalability of wet ball milling for the production of nanosuspensions, Pharm. Nanotechnol. 7 (2019) 147–161.
[18] H. Ueda, S. Aikawa, Y. Kashima, J. Kikuchi, Y. Ida, T. Tanino, K. Kadota, Y. Tozuka, Anti-plasticizing effect of amorphous indomethacin induced by specific intermolecular interactions with PVA copolymer, J. Pharm. Sci. 103 (2014) 2829–2838.
[19] K. Yuminoki, F. Seko, S. Horii, H. Takeuchi, K. Teramoto, Y. Nakada, N. Hashimoto, Application of povacoat as dispersion stabilizer of nanocrystal formulation, Asian J. Pharm. Sci. 11 (2016) 48–49.
[20] K. Yuminoki, F. Seko, S. Horii, H. Takeuchi, K. Teramoto, Y. Nakada, N. Hashimoto, Preparation and evaluation of high dispersion stable nanocrystal formulation of poorly water-soluble compounds by using Povacoat, J. Pharm. Sci. 103 (2014) 3772–3781.
[21] J. de Cássia Zaghi Compri, V.M. Andres Felli, F.R. Lourenço, T. Takatsuka, N. Fotaki, R. Löbenberg, N.A. Bou-Chacra, G.L. Barros de Araujo, Highly water-soluble orotic acid nanocrystals produced by high-energy milling, J. Pharm. Sci. 108 (2019) 1848–1856.
[22] United States Pharmacopeia and National Formulary, [USP 35 NF 30]. Buffer Solutions, (2011).
[23] G. Abate, R.N. Mshana, H. Miörner, Evaluation of a colorimetric assay based on (MTT) for rapid detection of rifampicin resistance in Mycobacterium tuberculosis, Int. J. Tuberc. Lung Dis. 2 (1998) 1011–1016.
[24] International Organization for Standartization, ISO 10993-5:2009 - Biological Evaluation of Medical Devices — Part 5: Tests for In Vitro Cytotoxicity, (2009).
[25] Douglas c. Montgomery, Introdução ao Controle Estatístico da Qualidade, 7a edição, Douglas c. Montgomery - Passei Direto, LTC, 2016.
[26] K.M. Raghava Srivalli, B. Mishra, Drug nanocrystals: a way toward scale-up, Saudi Pharm. J. 24 (2016) 386–404.
[27] Z.H. Loh, A.K. Samanta, P.W. Sia Heng, Overview of milling techniques for improving the solubility of poorly water-soluble drugs, Asian J. Pharm. Sci. 10 (2014) 255–274.
[28] M. Malamatari, K.M.G. Taylor, S. Malamataris, D. Douroumis, K. Kachrimanis, Pharmaceutical nanocrystals: production by wet milling and applications, Drug Discov. Today 23 (2018) 534–547.
[29] A.M. Cerdeira, M. Mazzotti, B. Gander, Miconazole nanosuspensions: influence of formulation variables on particle size reduction and physical stability, Int. J. Pharm. 396 (2010) 210–218.
[30] N. Jin, S.M. Pyo, C.M. Keck, R.H. Müller, Azithromycin nanocrystals for dermal prevention of tick bite infections, Pharmazie 74 (2019) 277–285.
[31] C.M. Keck, R.H. Müller, Size analysis of submicron particles by laser diffractometry-90% of the published measurements are false, Int. J. Pharm. 355 (2008) 150–163.
[32] J.S. Sohn, D.S. Yoon, J.Y. Sohn, J.S. Park, J.S. Choi, Development and evaluation of targeting ligands surface modified paclitaxel nanocrystals, Mater. Sci. Eng. C 72 (2017) 228–237.
[33] J.S. Choi, J.S. Park, Development of docetaxel nanocrystals surface modified with transferrin for tumor targeting, Drug Des. Devel. Ther. 11 (2017) 17–26.
[34] W. Abdelwahed, G. Degobert, S. Stainmesse, H. Fessi, Freeze-drying of nanoparticles: formulation, process and storage considerations☆, Adv. Drug Deliv. Rev. 58 (2006) 1688–1713.
[35] M.M. Chogale, V.N. Ghodake, V.B. Patravale, Performance parameters and characterizations of nanocrystals: a brief review, Pharmaceutics 8 (2016).
[36] R. Yadollahi, K. Vasilev, C.A. Prestidge, S. Simovic, Polymeric nanosuspensions for enhanced dissolution of water insoluble drugs, J. Nanomater. 2013 (2013) 1–10.
[37] G. Pelizza, M. Nebuloni, P. Ferrari, G.G. Gallo, Polymorphism of rifampicin, Farmaco. Sci. 32 (1977) 471–481.
[38] S. Agrawal, Y. Ashokraj, P.V. Bharatam, O. Pillai, R. Panchagnula, Solid-state characterization of rifampicin samples and its biopharmaceutic relevance, Eur. J. Pharm. Sci. 22 (2004) 127–144.
[39] D. Xia, P. Quan, H. Piao, H. Piao, S. Sun, Y. Yin, F. Cui, Preparation of stable nitrendipine nanosuspensions using the precipitation–ultrasonication method for enhancement of dissolution and oral bioavailability, Eur. J. Pharm. Sci. 40 (2010) 325–334.
[40] Y. Xu, X. Liu, R. Lian, S. Zheng, Z. Yin, Y. Lu, W. Wu, Enhanced dissolution and oral bioavailability of aripiprazole nanosuspensions prepared by nanoprecipitation/homogenization based on acid–base neutralization, Int. J. Pharm. 438 (2012) 287–295.
[41] E.P. Lavor, M.V.M. Navarro, F.D. Freire, C.F.S. Aragão, F.N. Raffin, E.G. Barbosa, T.F.A. De Lima, E. Moura, Application of thermal analysis to the study of anti-tuberculosis drugs-excipient compatibility, J. Therm. Anal. Calorim. 115 (2014) 2303–2309.
[42] A. Burger, J.O. Henck, S. Hetz, J.M. Rollinger, A.A. Weissnicht, H. Stöttner, Energy/temperature diagram and compression behavior of the polymorphs of D-mannitol, J. Pharm. Sci. 89 (2000) 457–468.
[43] J. Hecq, M. Deleers, D. Fanara, H. Vranckx, K. Amighi, Preparation and characterization of nanocrystals for solubility and dissolution rate enhancement of nifedipine, Int. J. Pharm. 299 (2005) 167–177.
[44] A. Sosnik, Á.M. Carcaboso, R.J. Glisoni, M.A. Moretton, D.A. Chiappetta, New old challenges in tuberculosis: potentially effective nanotechnologies in drug delivery, Adv. Drug Deliv. Rev. 62 (2010) 547–559.
[45] K.P. Krause, R.H. Müller, Production and characterisation of highly concentrated nanosuspensions by high pressure homogenisation, Int. J. Pharm. 214 (2001) 21–24.
[46] C. Rundfeldt, H. Steckel, H. Scherliess, E. Wyska, P. Wlaź, Inhalable highly concentrated itraconazole nanosuspension for the treatment of bronchopulmonary aspergillosis, Eur. J. Pharm. Biopharm. 83 (2013) 44–53.
[47] R.J. Prankerd, J.M. Walters, J.H. Parnes, Kinetics for degradation of rifampicin, an azomethine-containing drug which exhibits reversible hydrolysis in acidic solutions, Int. J. Pharm. 78 (1992) 59–67.
[48] K.C. Jindal, R.S. Chaudhary, A.K. Singla, S.S. Gangwal, S. Khanna, Dissolution test method for rifampicin—isoniazid fixed dose formulations, J. Pharm. Biomed. Anal. 12 (1994) 493–497.
[49] H.Ç. Arca, L.I. Mosquera-Giraldo, J.M. Pereira, N. Sriranganathan, L.S. Taylor, K.J. Edgar, Rifampin stability and solution concentration enhancement through amorphous solid dispersion in cellulose ω-carboxyalkanoate matrices, J. Pharm. Sci. 107 (2018) 127–138.
[50] L. Chen, Y. Wang, J. Zhang, L. Hao, H. Guo, H. Lou, D. Zhang, Bexarotene nanocrystal-oral and parenteral formulation development, characterization and pharmacokinetic evaluation, Eur. J. Pharm. Biopharm. 87 (2014) 160–169.
[51] A.A. Noyes, W.R. Whitney, The rate of solution of solid substances in their own solutions, J. Am. Chem. Soc. 19 (1897) 930–934.
[52] G. Buckton, A.E. Beezer, The relationship between particle size and solubility, Int. J. Pharm. 82 (1992) 7–10.
[53] T. Takatsuka, T. Endo, Y. Jianguo, K. Yuminoki, N. Hashimoto, Nanosizing of poorly water soluble compounds using rotation/revolution mixer, Chem. Pharm. Bull. (Tokyo) 57 (2009) 1061–1067.
[54] B. Sinha, R.H. Müller, J.P. Möschwitzer, Bottom-up approaches for preparing drug nanocrystals: formulations and factors affecting particle size, Int. J. Pharm. 453 (2013) 126–141.
[55] X. Zhai, J. Lademann, C.M. Keck, R.H. Müller, Dermal nanocrystals from medium soluble actives - physical stability and stability affecting parameters, Eur. J. Pharm. Biopharm. 88 (2014) 85–91.
[56] R. Shegokar, R.H. Müller, Nanocrystals: industrially feasible multifunctional formulation technology for poorly soluble actives, Int. J. Pharm. 399 (2010) 129–139.
[57] T. Liu, M. Han, F. Tian, D. Cun, J. Rantanen, M. Yang, Budesonide nanocrystal-loaded hyaluronic acid microparticles for inhalation: in vitro and in vivo evaluation, Carbohydr. Polym. 181 (2018) 1143–1152.
[58] R. Löbenberg, G.L. Amidon, H.G. Ferraz, N. Bou-Chacra, Mechanism of gastrointestinal drug absorption and application in therapeutic drug delivery, Ther. Deliv. Methods A Concise Overv. Emerg. Areas (2013) 8–22.
[59] V.B. Junyaprasert, B. Morakul, Nanocrystals for enhancement of oral bioavailability of poorly water-soluble drugs, Asian J. Pharm. Sci. 10 (2015) 13–23.
[60] R. Gadadare, L. Mandpe, V. Pokharkar, Ultra rapidly dissolving repaglinide nanosized crystals prepared via bottom-up and top-down approach: influence of food on pharmacokinetics behavior, AAPS PharmSciTech 16 (2015) 787–799.
[61] F. Lai, E. Pini, G. Angioni, M.L. Manca, J. Perricci, C. Sinico, A.M. Fadda, Nanocrystals as tool to improve piroxicam dissolution rate in novel orally disintegrating tablets, Eur. J. Pharm. Biopharm. 79 (2011) 552–558.
[62] M. Ochi, T. Kawachi, E. Toita, I. Hashimoto, K. Yuminoki, S. Onoue, N. Hashimoto, Development of nanocrystal formulation of meloxicam with improved dissolution and pharmacokinetic behaviors, Int. J. Pharm. 474 (2014) 151–156.
[63] G.L. Amidon, H. Lennernäs, V.P. Shah, J.R. Crison, A theoretical basis for a biopharmaceutic drug classification: the correlation of in vitro drug product dissolution and in vivo bioavailability, Pharm. Res. An Off. J. Am. Assoc. Pharm. Sci. 12 (1995) 413–420.
[64] S. Pourazar Dizaji, A. Taala, M. Masoumi, N. Ebrahimzadeh, A. Fateh, S.D. Siadat, F. Vaziri, Sub-minimum inhibitory concentration of rifampin: a potential risk factor for resuscitation of Mycobacterium tuberculosis, Antimicrob. Resist. Infect. Control 6 (2017) 1–5.
[65] H. Esmail, C.E. Barry, R.J. Wilkinson, Understanding latent tuberculosis: the key to improved diagnostic and novel treatment strategies, Drug Discov. Today 17 (2012) 514–521.
[66] A. Tuomela, J. Hirvonen, L. Peltonen, Stabilizing agents for drug nanocrystals: effect on bioavailability, Pharmaceutics 8 (2016).
[67] J.-Y. Choi, J.Y. Yoo, H.-S. Kwak, B. Uk Nam, J. Lee, Role of polymeric stabilizers for drug nanocrystal dispersions, Curr. Appl. Phys. 5 (2005) 472–474.
[68] S. Verma, S. Kumar, R. Gokhale, D.J. Burgess, Physical stability of nanosuspensions: investigation of the role of stabilizers on Ostwald ripening, Int. J. Pharm. 406 (2011) 145–152.
[69] T. Schön, P. Juréen, C.G. Giske, E. Chryssanthou, E. Sturegård, J. Werngren, G. Kahlmeter, S.E. Hoffner, K.A. Angeby, Evaluation of wild-type MIC distributions as a tool for determination of clinical breakpoints for Mycobacterium tuberculosis, J. Antimicrob. Chemother. 64 (2009) 786–793.
[70] T.L. Riss, R.A. Moravec, A.L. Niles, S. Duellman, H.A. Benink, T.J. Worzella,

L. Minor, Cell Viability Assays, Eli Lilly & Company and the National Center for Advancing Translational Sciences, 2004.
[71] G. Fotakis, J.A. Timbrell, In vitro cytotoxicity assays: comparison of LDH, neutral red, MTT and protein assay in hepatoma cell lines following exposure to cadmium chloride, Toxicol. Lett. 160 (2006) 171–177.
[72] Y. Wang, J. Rong, J. Zhang, Y. Liu, X. Meng, H. Guo, H. Liu, L. Chen, Morphology, in vivo distribution and antitumor activity of bexarotene nanocrystals in lung cancer, Drug Dev. Ind. Pharm. 43 (2017) 132–141.
[73] P.L. Reshma, B.S. Unnikrishnan, G.U. Preethi, H.P. Syama, M.G. Archana, K. Remya, R. Shiji, J. Sreekutty, T.T. Sreelekha, Overcoming drug-resistance in lung cancer cells by paclitaxel loaded galactoxyloglucan nanoparticles, Int. J. Biol. Macromol. 136 (2019) 266–274.
[74] A.R. Fernandes, J. Dias-Ferreira, C. Cabral, M.L. Garcia, E.B. Souto, Release kinetics and cell viability of ibuprofen nanocrystals produced by melt-emulsification, Colloids Surf. B: Biointerfaces 166 (2018) 24–28.